Human and Mouse Models for Kabuki Syndrome Reveal Increase in Inhibitory Synapse Development.

Short title: Altered synapse development in Kabuki syndrome

James Knopp[1], Alexander Weaver[1], Sean Miller[1], Toshihiro Nomura[2], Ava Whitlark[1], Jack Swantkowski[1], Alexandra Noble[1], Sandy Nam[1], Katharyn Hutson[1], Jenny Bergqvist-Patzke[1], Anis Contractor[2] and Christopher Patzke[1,*]

[1] Department of Biological Sciences, Boler-Parseghian Center for Rare Diseases, University of Notre Dame, Notre Dame, IN, USA

[2] Department of Neuroscience, Feinberg School of Medicine, Northwestern University, Chicago, Illinois, USA

*Address correspondence to: Christopher Patzke, 109A Galvin Life Science Center, University of Notre Dame, Notre Dame, IN 46556
Email: cpatzke@nd.edu

ABSTRACT

Intellectual disability, affecting 2-3% of the general population, often coincides with neurodevelopmental disorders and is frequently caused by mutations that impair synaptic function. Kabuki syndrome, a rare multisystem disorder associated with developmental delay and intellectual disability, results from mutations in either *KMT2D* (type 1) or *KDM6A* (type 2), which encode a chromatin-modifying methyltransferase and demethylase, respectively. However, the mechanisms contributing to intellectual disability in Kabuki syndrome remain poorly understood. In this study, we investigated synapse development in neurons using both *in vitro* human models of Kabuki syndrome types 1 and 2, as well as an *in vivo* mouse model of Kabuki syndrome type 1. Our findings revealed that both mature human iPSC-derived neurons and mice harboring disease-causing mutations exhibited increased inhibitory synapse development. This synaptic imbalance led to impaired excitatory information transfer within neural networks, which may underlie the cognitive deficits observed in Kabuki syndrome.

INTRODUCTION

Kabuki syndrome (KS) is a rare multisystem disorder associated with developmental delay and intellectual disability, affecting approximately 1 in 32,000 births. It is caused by mutations in either the *KMT2D* gene (KS type 1: 70% of cases) or the *KDM6A* gene (KS type 2: a small percentage of cases) [1]. *KMT2D* encodes a histone 3 lysine 4 mono-methylase (H3K4me1), while the X-linked KDM6A is a histone 3 lysine 27 trimethyl (H3K27me3) demethylase [2-7]. These enzymes are part of a protein complex in the cell nucleus that is associated with open chromatin states, thereby epigenetically regulating chromosomal gene expression.

KS affects the nervous system as well as the cardiovascular, skeletal-muscular, and digestive systems. It is characterized by distinct facial dysmorphism and up to 90% of affected individuals exhibit varying degrees of intellectual disability [8-11]. While reported animal studies elegantly revealed impaired neurogenesis in the hippocampus, associated memory defects [12-14], and improper cell differentiation [15,16], the mechanisms behind patients' intellectual disability symptoms remain largely unknown. Intellectual disability is often caused by mutations that developmentally impair synapses, neural cells and their circuits. Extensive work has been done to identify and understand mutations contributing to or causing intellectual disability [17-19]. For instance, previous research on the KS-related disorder Rubinstein-Taybi Syndrome has uncovered evidence of underlying synaptic deficits [20,21]. However, the specific effects in synaptic development and function underlying KS have not been investigated.

Here, we investigate the developmental consequences of engineered KS type 1 and KS type 2 Cre/lox-dependent loss-of-function mutations on synapse formation and function in human neurons, and KS type 1 in a mouse model. Our findings suggest that the KS mutations reduce excitatory synapse function while increasing inhibitory transmission thereby repressing information flow and coordinated network activity both *in vitro* and *in*

vivo. This conclusion is supported by morphological and functional changes, including alterations in synapse number, electrophysiological synaptic transmission and reduced network activity, as assessed by calcium imaging.

RESULTS

Heterozygous *Kmt2d* mutation leads to an increased number of inhibitory synapses in the mouse hippocampus

Because of their relevance as well-established disease model for KS type 1, we sought to investigate the effect of *Kmt2d* mutation on hippocampal synapses. We used heterozygous Kmt2d+/βGeo [12] mice to analyze synaptic morphology based on three different metrics: synaptic puncta density, puncta area, and puncta intensity, which reflect synapse number and clustering (Fig. 1A and 1B) [22]. We labeled neurons with the presynaptic pan-neuronal markers Synapsin and Bassoon and found increased puncta metrics in mutant neurons (Fig. 1C-F) with increases particularly at distances closest to the soma (Suppl. Fig. 1A-D). To determine whether this increase was specific to excitatory or inhibitory synapses, we performed labeling and measurements of vGlut1 (excitatory presynaptic marker) and vGAT (inhibitory presynaptic marker) on the same neurons. For vGlut1, no observed differences were between wild-type (WT) and mutant (Mut) groups in terms of puncta density; however, vGluT1 area and intensity were significantly decreased, suggesting that the *Kmt2d* mutation may lead to a deficit in excitatory presynaptic structures. In contrast, vGAT puncta measurements in mutant neurons showed an increase in density, area, and intensity, indicating an increase in inhibitory presynaptic structures in *Kmt2d*-mutant hippocampal neurons (Fig. 1G-J). In addition to presynaptic markers, we also measured synaptic puncta labeled by postsynaptic markers PSD95 (excitatory), and Gephyrin (inhibitory). PSD95 puncta were markedly reduced in density and intensity, while inhibitory postsynaptic Gephyrin density was significantly increased (Fig. 1K-L). Overall, these data suggest that *Kmt2d*-mutant mouse hippocampal neurons exhibit a marked increase in inhibitory synapse metrics, accompanied by a decrease in excitatory parameters.

Kmt2d mutation decreases the overall number of hippocampal neurons but does not affect the number of inhibitory neurons

Because *Kmt2d*, essential for enhancer activation, is associated with defects in cell-type specific gene expression and cell differentiation, we next tested whether the number of neurons from mutant hippocampi was altered. We counted WT and Mut neurons as Map2- and DAPI-positive cells and detected a slight decrease in the mutant condition, consistent with previous work [12]. Glial cell numbers (Map2-negative cells) did not

change (Fig. 2 A-C). Interestingly, mutant neurons displayed longer dendrites with no alterations in the number of processes, branches, and the cell body area (Suppl. Fig. 1F-I). To determine whether the observed increase in inhibitory synapses in mutant neurons was due to an increased number of inhibitory neurons or the same number of inhibitory forming more synapses, we examined the markers Somatostatin, Parvalbumin, and Necab1 – all of which label inhibitory neurons – and detected no changes Fig. 2D-G). This suggests that the same number of inhibitory neurons forms more synapses in *Kmt2d*-mutant neurons.

***Kmt2d* mutation leads to decreased calcium activity in mouse hippocampal neurons.**

To better understand the functional consequences of increased inhibitory synaptic development on the neural networks of *Kmt2d*-mutant neurons, we performed GCaMP8m-based calcium imaging (Fig. 2H and I). Our analysis revealed decreased event frequencies in individual mutant neurons, along with increased amplitudes. The synchronous (average) frequency was not changed (Fig. 2J-L). Together, these findings indicate that network activity is reduced, confirming the physiological relevance of the KS type 1 mutation.

Kmt2d* mutation results in increased number of functional inhibitory synapses *in vivo

To test whether the inhibitory phenotype observed *in vitro* is also present *in vivo*, we performed immunohistochemistry on horizontal brain sections from young adult mice (postnatal day 30) followed by confocal imaging of the hippocampal region. Consistent with our *in vitro* data, we detected a significant increase in vGAT intensity in mutant hippocampi. No difference in vGluT1 intensity was observed when compared to wild-type hippocampi (Fig. 3A-E and Suppl. Fig. 2). Thus, our data confirm that the increase of inhibitory synapses in mutant mice is relevant to hippocampal *in vivo* development. Next, we investigated the physiological consequence of increased inhibitory synapse formation in *Kmt2d*-mutant mice by recording excitatory (EPSCs) and inhibitory postsynaptic currents (IPSCs) from pyramidal neurons after stimulation of Schaffer collaterals (Fig. 3F). IPSCs and EPSCs were recorded from the same neurons. The ratio of IPSC amplitude to EPSC amplitude (I/E ratio) was measured in each cell and was compared between genotypes (WT and Mut). The I/E ratio was significantly higher in mutant mice (WT: 137.7 ± 11.6 %; Mut: 210.3 ± 21.2 %). In summary, the data from *Kmt2d*-mutant mice show that the development of inhibitory synapses is increased in this model for KS type 1.

Increased number of inhibitory synapses in a human model for Kabuki syndrome type 1

In humans, the *KMT2D* gene is located on chromosome 12 and is over 19 kilobase pairs in length containing 54 exons. To model KS type 1 in human cells, we engineered a heterozygous conditional knockout targeting exon 6 of *KMT2D* in human induced pluripotent stem cells (iPSCs) derived from a donor without disease-causing mutations. We then directly differentiated these cells by forced expression of *Ngn2* [23], to produce purely excitatory neurons, or produced purely inhibitory neurons by expression of *Ascl1* and *Dlx2* [24] (Suppl. Fig. 3). The mutation was induced via co-expression of Cre-recombinase. As a wild-type control, we used cells treated with an inactive mutant ΔCre (Fig. 4A-D). Excitatory mutant neurons exhibited a drastic decrease in the density of PSD95-positive puncta, while inhibitory neurons derived from the same cells displayed an increase in vGAT puncta density when compared to ΔCre-treated neurons (Fig. 4E-H), suggesting that *KMT2D*-mutant human neurons exhibit similar phenotypes to *Kmt2d*-mutant mice. To determine the functional consequences of the *KMT2D* mutation, we performed calcium imaging experiments. In order to observe coordinated circuit activity, we chose to examine excitatory human neurons. We observed the same effect as seen in mouse hippocampal neurons: a decreased single-neuron event frequency in the mutant condition with higher signal amplitude but no differences in synchronous (average) frequency (Fig. 4I-M). Together, these data suggest that our human model system recapitulates the KS type 1 mutation phenotype of the mouse model with a marked increase in inhibitory synapse formation.

Increased inhibitory synaptic puncta parameters in a human model for Kabuki syndrome type 2

Next, we asked whether induction of KS type 2 in human neurons would cause the same effect as observed in the mouse and human KS type 1 model systems. We flanked exon 7 of the *KDM6A* gene with loxP sites in otherwise wild-type iPSCs derived from a male donor (same donor as used for our human KS type 1 model) (Fig. 5A). Cre-expression led to deletion of detectable KDM6A signal in immunocytochemistry (Fig. 5B). In parallel with the induction of the KS type 2-causing mutation by treatment with Cre, we differentiated these engineered cells into inhibitory human neurons, labeled inhibitory synapses for vGAT, and detected an increase in synaptic puncta metrics (Fig. 5C-E). Next, we performed calcium imaging to assess network activity. Strikingly, we observed a decrease in single-neuron and synchronous calcium transient frequency, along with an increase in signal amplitudes in *KDM6A*-mutant neurons (Fig. 5F-K). Overall, the phenotype of *KDM6A*-mutant human neurons is similar to the phenotypes observed *KMT2D*-mutant human and mouse neurons.

DISCUSSION

Our findings demonstrate a novel imbalance between excitatory and inhibitory synaptic processes in a well-characterized mouse model of KS type 1. This imbalance is caused by increases in the number of inhibitory synapses, as shown by elevated levels of vGAT and Gephyrin in cultured hippocampal neurons as well as elevated vGAT in immunohistology of mouse brain slices. In cultures, no differences were observed for vGluT1 density. However, a significant reduction was observed in vGluT1 puncta size and intensity, suggesting that *Kmt2d* mutation may lead to reduced clusters of excitatory synapses, and therefore a change in the number of presynaptic structures. In addition, a reduction in PSD95 was observed, suggesting a potential decrease in excitatory synapses. These data suggest that the *Kmt2d* mutation changes the overall development of synapses and skews the balance toward inhibitory synaptic dominance. Strikingly, these observations in mice are backed up by our newly created Cre/lox-mediated human neuron model systems for KS type 1 and type 2. The recurring detection of increased inhibitory synapse formation in all three model systems (mouse KS type 1, human KS type 1, and human KS type 2) is a central theme in mutant neurons.

In summary, our results suggest that KS-causing mutations enahnce inhibitory synaptic transmission while reducing excitatory synaptic transmission, and the resulting imbalance in neuronal inhibition to excitation represses information flow and coordinated network activity (Fig. 6). This conclusion is supported by morphological and functional changes, including changes in the number of synapses, changes in electrophysiological recordings, and alterations in calcium event frequency. The combined increase in inhibitory synaptic markers and decrease in excitatory synaptic markers, coupled with alterations in synaptic currents and calcium activity, suggest that aberrant synaptic function is the underlying cause for the intellectual disability associated with Kabuki Syndrome. These findings could help to inform the development of targeted treatments and therapies aimed at rescuing I/E imbalance in affected individuals.

The molecular basis of the observed synaptic changes in KS are likely rooted in the chromatin remodeling functions of both KMT2D and KDM6A. Mutations in *KMT2D* are known to disrupt histone methylation, altering gene expression (**citations**). Our results suggest that *KMT2D* and *KDM6A* loss-of-function mutations may lead to the repression of transcriptional programs necessary for maintaining a balanced level of excitatory and inhibitory synapses.

Restoration of excitatory and inhibitory synaptic balance presents a promising therapeutic strategy for KS. In particular, pharmacological interventions that increase excitatory synaptic activity or decrease excessive inhibitory synaptic activity could help to rescue synaptic homeostasis. Several drugs which have been shown to enhance AMPA (Aniracetam, Piracetam) and NMDA (D-cycloserine) receptor activity as well as

those shown to decrease GABA-A (Bicuculline, Gabazine) or GABA-B (CGP55845) receptor activity would serve as prime tools for studies involving the pharmacological modulation of the I/E imbalance and for determining potential targets in treating Kabuki syndrome. Ultimately, our findings lay the foundation for development of treatments designed to target the synaptic basis of intellectual disability in KS and potentially other similar disorders.

MATERIALS AND METHODS

Mice: Animal experiments conducted in this study were in accordance with National Institute of Health Guidelines for the Care and Use of Laboratory Mice and approved by the Institutional Animal Care and Use Committee (IACUC) at the University of Notre Dame. The Kmt2d+/βGeo mice used in this study were originally generated at Bay Genomics and then back-crossed for several generations to obtain line stability. An expression cassette encoding a β-galactosidase neomycin resistance fusion protein (βGeo) was inserted into intron 50 of *Kmt2d* on mouse chromosome 15 and is predicted to generate a truncated Kmt2d protein with peptide sequence corresponding to the first 50 exons of *Kmt2d* fused to βGeo, but lacking the SET domain and therefore methyltransferase activity [12]. For breeding of Kmt2d+/βGeo mice, matings were set up using a heterozygous male and WT female. For all analyses, littermates were used.

Mouse hippocampal cultures: To generate cultured mouse hippocampal neurons, brains were dissected from P0 mice and rinsed quickly with ice-cold Hank's Balanced Buffered Saline (HBSS) before continued dissection of the hippocampus, digestion with papain, and then seeding onto matrigel-coated coverslips in MEM medium (ThermoFisher Scientific). P0 was defined as the day the pups were born. On day in vitro (DIV) 1, the medium was changed to neurobasal medium containing B27. On DIV3, the medium was exchanged for medium containing 2 μM AraC, and cells were infected with lentiviruses that encoded GCaMP8m. Calcium imaging or immunostaining was performed at DIV14–16, when the cells are considered mature.

Immunofluorescent labeling of hippocampus: For immunohistochemistry, P30 mice were perfused with phosphate-buffered saline (PBS) and then PBS containing 4% PFA. Brains were dissected and rinsed quickly in ice-cold PBS before soaking in 30% sucrose. Brain tissues were embedded in optimal cutting temperature compound (OCT, Tissue Plus, Fisher) with embedding mold and frozen on dry ice. Embedded brain samples were stored at −80°C until further use. To sample the hippocampus in horizontal planes, multiple dorsal-ventral (horizontal) cryosections with a thickness of 30 um were collected. Brain sections were sliced using a cryostat (Leica Microsystems, CM3050-S) and then blocked using a solution containing goat serum and Triton-X100. Immunostaining was performed on slices while free-floating. Individual slices were mounted manually onto superfrost slides (VWR) using a paint brush.

Calcium imaging: Calcium imaging was performed as previously described [25,26]. Coverslips were gently placed into a dark imaging chamber with an open bottom and then washed twice with a washing buffer before time-lapse imaging was performed in calcium-imaging buffer. After 1–2 min equilibration in a 37°C incubator, calcium-imaging was performed on an inverted epi-fluorescence microscope (Nikon EclipseTS2R) with a 488 nm filter at room temperature. GCaMP8m fluorescence was recorded for 2 min at a frame rate of 9-10 frames/s. Approximately 1000-3000 time-lapse images were acquired at a 1 × digital zoom using a 20x objective. For each condition, 4-5 fields of view were imaged per coverslip and a minimal 2 coverslips were used for each biological batch. All images were acquired using the same exposure time. Time-lapse imaging was performed in areas containing confluent neuron populations with few overlapping cell somata.

Hippocampal slice electrophysiology: Mice were anesthetized with isoflurane followed by ketamine/xylazine, then rapid cardiac perfusion was performed using ice-cold sucrose artificial cerebrospinal fluid (ACSF) containing the following (in mM): 85 NaCl, 2.5 KCl, 1.25 NaH2PO4, 25 NaHCO3, 25 glucose, 75 sucrose, 0.5 CaCl2, and 4 MgCl2, equilibrated with 95% O2/5% CO2 before mice were decapitated. Brains were rapidly removed and placed in the same ice-cold sucrose ACSF as described above. Coronal hippocampal slices (250 µm thick) were prepared using a Leica VT1000S or VT1200 S vibratome and transferred to a heated (28-32°C) holding chamber containing the same sucrose ACSF, which was gradually exchanged for regular ACSF containing the following (in mM): 125 NaCl, 2.5 KCl, 1.25 NaH2PO4, 25 NaHCO3, 25 glucose, 2 CaCl2, and 1 MgCl2, equilibrated with 95% O2/5% CO2 at room temperature. After incubation in regular ACSF for at least one hour, slices were transferred to a recording chamber and perfused continuously with oxygenated regular ACSF at a flow rate of 2 ml/min.

Excitatory and inhibitory postsynaptic currents (EPSCs and IPSCs) were recorded from pyramidal neurons in the CA1 subregion of the hippocampus. Stimulating electrodes were placed in the stratum radiatum to stimulate Schaffer collaterals from the CA3 neurons. EPSCs and IPSCs were isolated by switching the holding voltage at -50 mV and at 0 mV, which are close to the reversal potentials for Cl- and Na+ [27]. Stimulation intensity was adjusted to evoke EPSCs with amplitudes of 300- 400 pA in individual neurons, and then IPSCs were recorded from the same neurons. The ratio of IPSC amplitude to EPSC amplitude (I to E ratio) was measured in each cell and was compared between genotypes (WT and Het).

Viral constructs. The following lentiviral constructs were used: 1. FUW-TetO-Ngn2-T2A-puromycin (TetO promoter drives expression of full-length mouse Ngn2 and of puromycin via the cleavage-peptide sequence T2A). 2. FUW-rtTA. 3. FUW-GFP::Cre to express Cre-recombinase or GFP::ΔCre for the wild-type control. 6. FUW-GCaMP8m for Ca^{2+} imaging.

Virus generation. Lentiviruses were produced as described [23] in HEK293T cells (ATCC, VA) by co-transfection with three helper plasmids (pRSV-REV, pMDLg/pRRE and vesicular stomatitis virus G protein expression vector) with 12 µg of lentiviral vector DNA and 6 µg of each of the helper plasmid DNA per 75 cm^2 culture area) using calcium phosphate. Lentiviruses were harvested in the medium 48 h after transfection, aliquoted, and frozen at -80ºC.

Cell culture. Experiments were performed as follows. 1019 iPSCs (ATCC-DYS0100 Human Induced Pluripotent Stem (IPS) Cells) were maintained as feeder-free cells in Stemflex medium (Thermo). Mouse glial cells were cultured from the forebrain of new-born wild-type CD1 mice. Briefly, new-born mouse forebrain homogenates were digested with papain and EDTA for 15 min, cells were dissociated by harsh trituration to avoid growing of neurons, and plated onto T75 flasks in DMEM supplemented with 10% FBS. Upon reaching confluence, glial cells were trypsinized and replated at lower density a total of two times to remove potential trace amounts of mouse neurons before the glia cell cultures were used for co-culture experiment with human neurons.

Standard protocol for generation of neurons from conditional mutant human iPS cells and for activating the conditional mutations. Human neuron generation has been described previously [23]. Briefly, targeted human iPSCs were treated with Accutase (Innovative Cell Technologies) and plated as dissociated cells in 24-well plates (1 x 10^4 cells/well) on day -1. Cells were plated on matrigel (BD Biosciences)-coated coverslips in Stemflex containing 2 mM thiazovivin (Bio Vision). At the same time point, lentiviruses were prepared as described above and added to each well (14 µl/well of 24-well plate) in a total volume of 500 µl. Mainly two different types of lentiviruses were used for co-infection: the lentiviruses used for human neuron induction as described, and lentiviruses expressing either Cre-recombinase (to create a null allele) under control of the ubiquitin promoter or an inactive mutated ΔCre-recombinase for the wild-type control. On day 0, the culture medium was replaced with N2/DMEM/F12/NEAA (Invitrogen) containing human BDNF (10 ng/ml, PeproTech), human NT-3 (10 ng/ml, PeproTech), and mouse Laminin-1 (0.2 µg/ml, Invitrogen). Doxycycline (2 µg/ml, Clontech) was added on day 0 to induce TetO gene expression and retained in the medium until the end of the experiment. On day 1, a 24 hr puromycin selection (1 µg/ml) period was started. On day 2, mouse glia cells were added in neurobasal medium supplemented with B27/Glutamax (Invitrogen) containing BDNF, NT3 and Laminin-1; Ara-C (2 µM, Sigma) was added to the medium to inhibit glial proliferation. After day 2, 50% of the medium in each well was exchanged every 2 days. FBS (5%) was added to the culture medium on day 10 to support astrocyte viability, and human neurons were assayed after at least 2 (excitatory) or 4 (inhibitory) months or as indicated.

Data presentation and statistics. Part of Figures 1B, 3F, and 6, were created with BioRender.com. All data shown are individual values and means ± SEMs; Number of measured cells and/or independent experiments is indicated inside each bar or mentioned in the figure. All statistical analyses were performed using r unpaired two-tailed Student's t-test (when two experimental were compared to each other) comparing the test sample to the control sample examined in the same experiments. No power analysis were performed to predetermine sample sizes. Our sample sizes are similar to those generally employed in the field. Sample allocation was random. We did not test for normal distribution.

AKNOWLEDGEMENTS

This work was supported by funds from the University of Notre, the Brain foundation to C.P. We thank Dr. Kasturi Haldar for sharing the Kmt2d+/βGeo mice with us. We thank the undergraduate summer students Isabella Wiebelt-Smith and Jeremiah Lopez for helping with the synapse binning experiment and counting neurons.

CONFLICT OF INTEREST

The authors declare no competing financial interests.

AUTHOR CONTRIBUTIONS

C.P. conceived the study. C.P. and J.K., designed most of the experiments. J.K., A.W., S.M., A.W., J.S., A.N., K.H., J.B.-P., and S.N. performed and analyzed most of the experiments. T.N., and A.C. contributed to specific experiments. C.P. and J.K. prepared the manuscript with input from all authors.

REFERENCES

1 Boniel, S., Szymańska, K., Śmigiel, R. & Szczałuba, K. Kabuki Syndrome-Clinical Review with Molecular Aspects. *Genes (Basel)* **12**, doi:10.3390/genes12040468 (2021).
2 Li, Y. *et al.* A mutation screen in patients with Kabuki syndrome. *Hum Genet* **130**, 715-724, doi:10.1007/s00439-011-1004-y (2011).
3 Ng, S. B. *et al.* Exome sequencing identifies MLL2 mutations as a cause of Kabuki syndrome. *Nature genetics* **42**, 790-793, doi:10.1038/ng.646 (2010).
4 Miyake, N. *et al.* KDM6A point mutations cause Kabuki syndrome. *Human mutation* **34**, 108-110, doi:10.1002/humu.22229 (2013).
5 Agger, K. *et al.* UTX and JMJD3 are histone H3K27 demethylases involved in HOX gene regulation and development. *Nature* **449**, 731-734, doi:10.1038/nature06145 (2007).
6 Lee, J. E. *et al.* H3K4 mono- and di-methyltransferase MLL4 is required for enhancer activation during cell differentiation. *Elife* **2**, e01503, doi:10.7554/eLife.01503 (2013).

7 Lan, F. *et al.* A histone H3 lysine 27 demethylase regulates animal posterior development. *Nature* **449**, 689-694, doi:10.1038/nature06192 (2007).
8 Niikawa, N. *et al.* Kabuki make-up (Niikawa-Kuroki) syndrome: a study of 62 patients. *Am J Med Genet* **31**, 565-589, doi:10.1002/ajmg.1320310312 (1988).
9 Hannibal, M. C. *et al.* Spectrum of MLL2 (ALR) mutations in 110 cases of Kabuki syndrome. *American journal of medical genetics. Part A* **155a**, 1511-1516, doi:10.1002/ajmg.a.34074 (2011).
10 Bögershausen, N. & Wollnik, B. Unmasking Kabuki syndrome. *Clin Genet* **83**, 201-211, doi:10.1111/cge.12051 (2013).
11 Paulussen, A. D. *et al.* MLL2 mutation spectrum in 45 patients with Kabuki syndrome. *Human mutation* **32**, E2018-2025, doi:10.1002/humu.21416 (2011).
12 Bjornsson, H. T. *et al.* Histone deacetylase inhibition rescues structural and functional brain deficits in a mouse model of Kabuki syndrome. *Science translational medicine* **6**, 256ra135, doi:10.1126/scitranslmed.3009278 (2014).
13 Carosso, G. A. *et al.* Precocious neuronal differentiation and disrupted oxygen responses in Kabuki syndrome. *JCI Insight* **4**, doi:10.1172/jci.insight.129375 (2019).
14 Benjamin, J. S. *et al.* A ketogenic diet rescues hippocampal memory defects in a mouse model of Kabuki syndrome. *Proceedings of the National Academy of Sciences* **114**, 125-130, doi:doi:10.1073/pnas.1611431114 (2017).
15 Schwenty-Lara, J., Nehl, D. & Borchers, A. The histone methyltransferase KMT2D, mutated in Kabuki syndrome patients, is required for neural crest cell formation and migration. *Human molecular genetics* **29**, 305-319, doi:10.1093/hmg/ddz284 (2020).
16 Van Laarhoven, P. M. *et al.* Kabuki syndrome genes KMT2D and KDM6A: functional analyses demonstrate critical roles in craniofacial, heart and brain development. *Human molecular genetics* **24**, 4443-4453, doi:10.1093/hmg/ddv180 (2015).
17 Zoghbi, H. Y. & Bear, M. F. Synaptic dysfunction in neurodevelopmental disorders associated with autism and intellectual disabilities. *Cold Spring Harbor perspectives in biology* **4**, doi:10.1101/cshperspect.a009886 (2012).
18 Srivastava, A. K. & Schwartz, C. E. Intellectual disability and autism spectrum disorders: causal genes and molecular mechanisms. *Neurosci Biobehav Rev* **46 Pt 2**, 161-174, doi:10.1016/j.neubiorev.2014.02.015 (2014).
19 Sullivan, P. F. & Geschwind, D. H. Defining the Genetic, Genomic, Cellular, and Diagnostic Architectures of Psychiatric Disorders. *Cell* **177**, 162-183, doi:10.1016/j.cell.2019.01.015 (2019).
20 de Thonel, A. *et al.* CBP-HSF2 structural and functional interplay in Rubinstein-Taybi neurodevelopmental disorder. *Nature communications* **13**, 7002, doi:10.1038/s41467-022-34476-2 (2022).
21 Lintas, C. & Persico, A. M. Unraveling molecular pathways shared by Kabuki and Kabuki-like syndromes. *Clin Genet* **94**, 283-295, doi:10.1111/cge.12983 (2018).
22 Patzke, C. *et al.* Neuromodulator Signaling Bidirectionally Controls Vesicle Numbers in Human Synapses. *Cell* **179**, 498-513 e422, doi:10.1016/j.cell.2019.09.011 (2019).
23 Zhang, Y. *et al.* Rapid Single-Step Induction of Functional Neurons from Human Pluripotent Stem Cells. *Neuron* **78**, 785-798, doi:http://dx.doi.org/10.1016/j.neuron.2013.05.029 (2013).
24 Yang, N. *et al.* Generation of oligodendroglial cells by direct lineage conversion. *Nature biotechnology* **31**, 434-439, doi:10.1038/nbt.2564 (2013).
25 Patzke, C. *et al.* Cannabinoid receptor activation acutely increases synaptic vesicle numbers by activating synapsins in human synapses. *Molecular psychiatry*, doi:10.1038/s41380-021-01095-0 (2021).

26 Sun, Z. & Südhof, T. C. A simple Ca(2+)-imaging approach to neural network analyses in cultured neurons. *Journal of neuroscience methods* **349**, 109041, doi:10.1016/j.jneumeth.2020.109041 (2021).
27 Kourdougli, N. *et al.* The NKCC1 Inhibitor Bumetanide Restores Cortical Feedforward Inhibition and Lessens Sensory Hypersensitivity in Early Postnatal Fragile X Mice. *Biological psychiatry*, doi:10.1016/j.biopsych.2024.06.023 (2024).

FIGURES AND FIGURE LEGENDS – Knopp et al. 2024

Fig.1

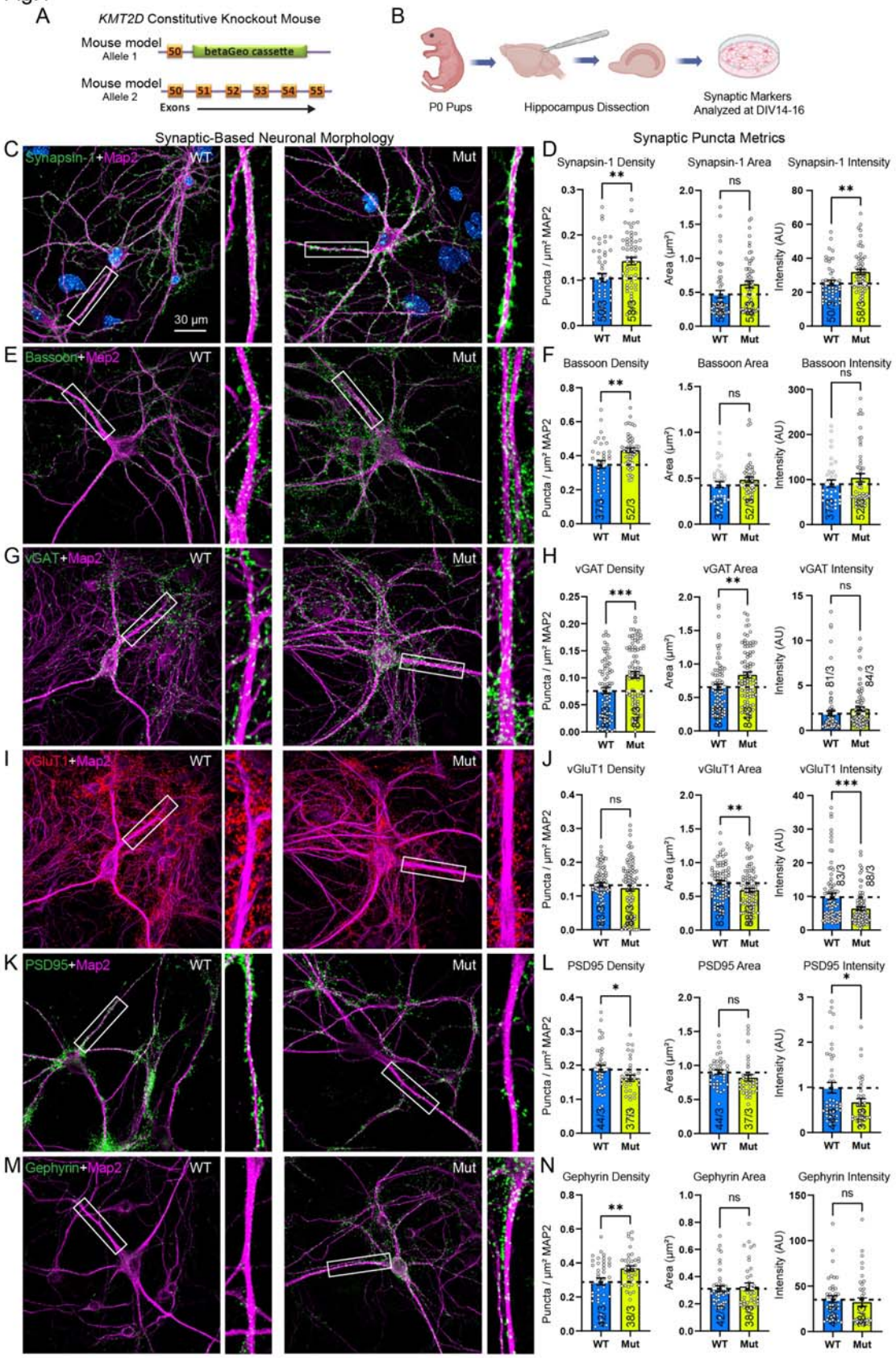
A
KMT2D Constitutive Knockout Mouse
Mouse model Allele 1
50
betaGeo cassette
Mouse model Allele 2
50 51 52 53 54 55
Exons
B
P0 Pups
Hippocampus Dissection
Synaptic Markers Analyzed at DIV14-16
Synaptic-Based Neuronal Morphology
Synaptic Puncta Metrics
C Synapsin-1+Map2 WT Mut
30 µm
D Synapsin-1 Density
Synapsin-1 Area
Synapsin-1 Intensity
E Bassoon+Map2 WT Mut
F Bassoon Density
Bassoon Area
Bassoon Intensity
G vGAT+Map2 WT Mut
H vGAT Density
vGAT Area
vGAT Intensity
I vGluT1+Map2 WT Mut
J vGluT1 Density
vGluT1 Area
vGluT1 Intensity
K PSD95+Map2 WT Mut
L PSD95 Density
PSD95 Area
PSD95 Intensity
M Gephyrin+Map2 WT Mut
N Gephyrin Density
Gephyrin Area
Gephyrin Intensity
Puncta / µm² MAP2
Area (µm²)
Intensity (AU)
WT
Mut
ns

Figure 1: Increased development of inhibitory synapses in a mouse model for Kabuki syndrome type 1

A and B, Schematic rationale of experiments: Newborn P0 mouse pups (littermates with (Mut) and without (WT) heterozygous mutation) were used to analyze synaptic puncta metrics in hippocampal cells.

C and D, Immunocytochemistry images showing synaptic morphology labeled for presynaptic Synapsin-1 (green), Map2 (magenta), and DAPI (blue). A zoomed-in view is included. Summary graphs show synaptic puncta density, puncta area and intensity for Synapsins-1.

E and F, Immunocytochemistry images showing synaptic morphology labeled for presynaptic Bassoon (green), Map2 (magenta), and DAPI (blue). A zoomed-in view is included. Summary graphs show synaptic puncta densities, puncta area and intensities for Bassoon.

G - I, Immunocytochemistry images of the same cells showing synaptic morphology of presynaptic excitatory vGluT1 (G) and inhibitory vGAT (I) synapses. H and J, Summary graphs show synaptic puncta density, puncta area and intensity.

K and L, Immunocytochemistry images showing synaptic morphology labeled for postsynaptic excitatory PSD95 (green), Map2 (magenta), and DAPI (blue). A zoomed-in view is included. Summary graphs show synaptic puncta densities, puncta area and intensities for PSD95.

M and N, Immunocytochemistry images showing synaptic-based morphology labeled for postsynaptic inhibitory Gephyrin (green), Map2 (magenta), and DAPI (blue). A zoomed-in view is included. Summary graphs show synaptic puncta densities, puncta area and intensities for Gephyrin.

Data are presented as individual values (each representing one image) and means ± SEM; statistical significance was assessed by two-tailed unpaired Student's t-test (*, $P < 0.05$; **, $P < 0.01$; *** $p<0.001$).

Fig.2

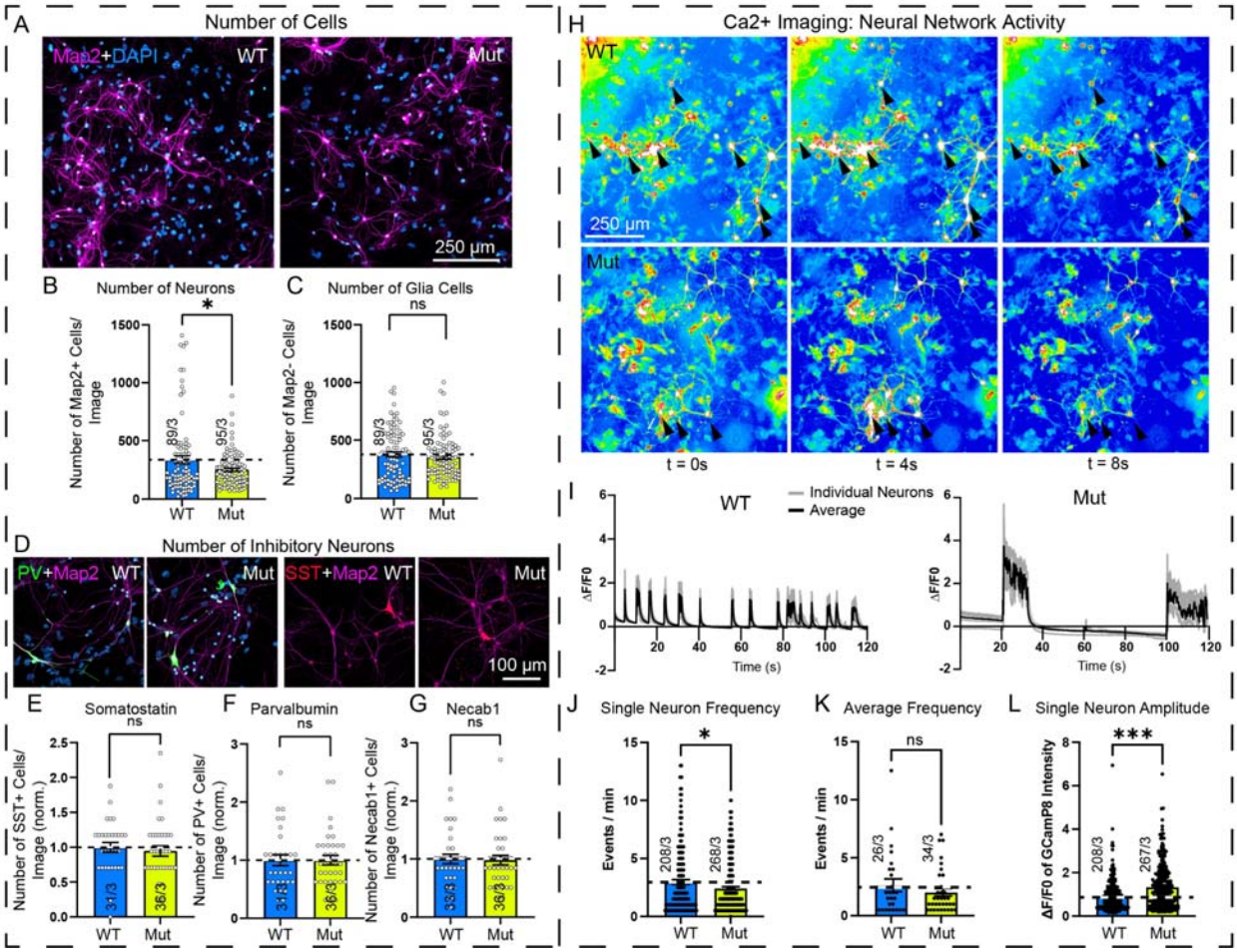

Figure 2. Kmt2d mutation in mice leads to decreased neuronal calcium activity but no change in the number of inhibitory neurons.

A-C, Representative micrographs of WT and Mut hippocampal cells. Neuronal numbers were assessed by Map2-positive somata. Map2-negative cells were considered glia cells.

D-G, Representative micrographs showing WT and Mut hippocampal cells stained for inhibitory neuronal markers Somatostatin (SST) and Parvalbumin (PV). Summary graphs quantify the relative (to WT) number of positive cells, including the inhibitory neuronal marker Necab1.

H, Representative calcium imaging micrographs of cultured wild-type (WT) and mutant (Mut) mouse hippocampal neurons overexpressing GCaMP8. Network activity was induced with 2.5 mM KCl and 2 mM $CaCl_2$. Warmer colors indicate higher fluorescence intensity. Arrows highlight active neurons showing calcium transients.

I, Representative traces of GCaMP8 transients. Fluorescence intensity changes (ΔF/F0) over time reveal a more clustered pattern and higher signal intensities in Mut neurons.

J-L, Summary graphs showing individual neuron firing frequency (J), average firing frequency per view field (K), and signal intensities in single neurons (L).

Data are presented as individual values (one movie or image in B, C, E, F, G, K ; and one cell in J and L) and means ± SEM; statistical significance was assessed by two-tailed unpaired Student's t-test (*, $P < 0.05$; *** $p<0.001$).

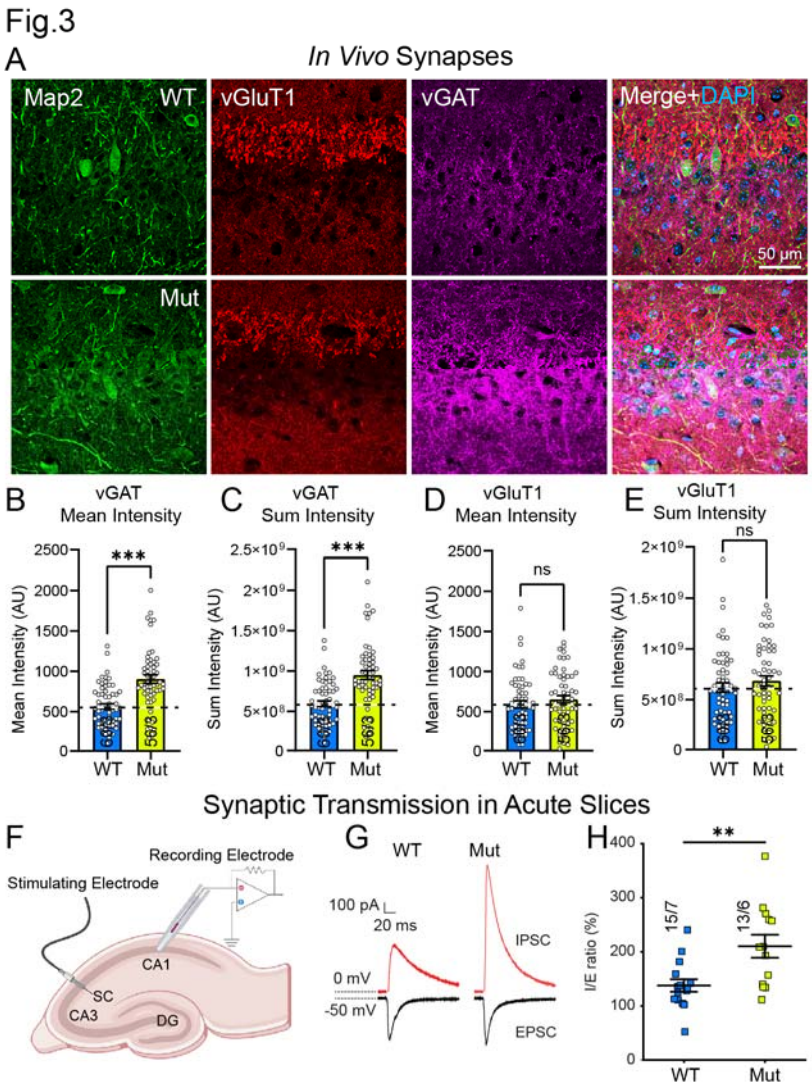

Figure 3: Increased number of functional inhibitory synapses in vivo.

A, Representative micrographs of hippocampal sections showing the CA3 region of WT and Mut mice. Sections are stained for Map2 (green), vGluT1 (red), vGAT (magenta), and Dapi (blue).

B-E, Summary graphs for vGAT and vGluT1 staining showing mean instensity (intensity of all pixels/number of pixels) and the sum intensity of all pixels with the field of view.

F, Experimental paradigm for recordings from acute hippocampal slices of WT and Mut mice.

G and H, Representative traces of evoked IPSC (I) and EPSC (E) amplitudes and the summary graph showing their ratios. WT: 15 cells from 7 mice; Mut: 13 cells from 6 mice were recorded.

Data are individual values (one image in B-E; and one cell in H) and means ± SEM; statistical significance was assessed by two-tailed unpaired Student's t-test (**, $P < 0.01$; *** $p<0.001$).

Fig.4

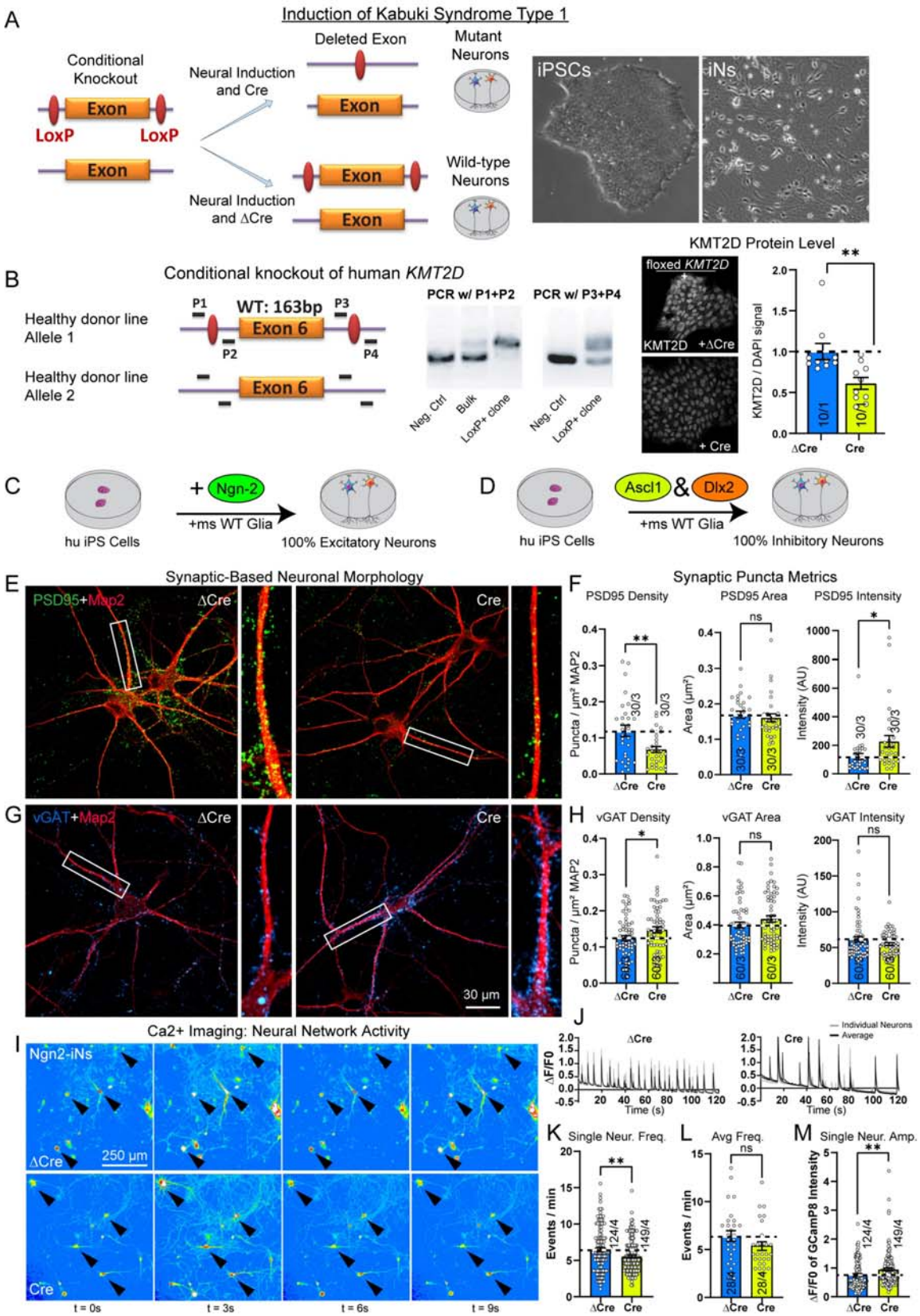
A
Induction of Kabuki Syndrome Type 1
Conditional Knockout
Exon
LoxP
LoxP
Exon
Neural Induction and Cre
Deleted Exon
Exon
Mutant Neurons
Neural Induction and ΔCre
Exon
Exon
Wild-type Neurons
iPSCs
iNs
B
Conditional knockout of human KMT2D
Healthy donor line Allele 1
Healthy donor line Allele 2
P1
WT: 163bp
P3
Exon 6
P2
P4
Exon 6
PCR w/ P1+P2
PCR w/ P3+P4
Neg. Ctrl
Bulk
LoxP+ clone
Neg. Ctrl
LoxP+ clone
floxed KMT2D
KMT2D +ΔCre
+ Cre
KMT2D Protein Level
KMT2D / DAPI signal
10/1
10/1
ΔCre
Cre
C
hu iPS Cells
+ Ngn-2
+ms WT Glia
100% Excitatory Neurons
D
hu iPS Cells
Ascl1 & Dlx2
+ms WT Glia
100% Inhibitory Neurons
E
Synaptic-Based Neuronal Morphology
PSD95+Map2
ΔCre
Cre
F
Synaptic Puncta Metrics
PSD95 Density
PSD95 Area
PSD95 Intensity
Puncta / µm² MAP2
Area (µm²)
Intensity (AU)
30/3
30/3
ΔCre
Cre
G
vGAT+Map2
ΔCre
Cre
30 µm
H
vGAT Density
vGAT Area
vGAT Intensity
60/3
60/3
I
Ca2+ Imaging: Neural Network Activity
Ngn2-iNs
ΔCre
250 µm
Cre
t = 0s
t = 3s
t = 6s
t = 9s
J
ΔCre
Cre
Individual Neurons
Average
ΔF/F0
Time (s)
K
Single Neur. Freq.
Events / min
124/4
149/4
L
Avg Freq.
28/4
28/4
M
Single Neur. Amp.
ΔF/F0 of GCamP8 Intensity
124/4
149/4

Figure 4: Increased number of inhibitory synapses in a human model for Kabuki syndrome type 1

A, General strategy for Cre/loxP-mediated induction of Kabuki syndrome type1 in human iPSCs from a donor without disease-causing mutations, and their differentiation into purely isogenic wild-type and mutant induced neurons (iNs).

B, Specific heterozygous targeting of *KMT2D* and PCR- based screening strategy for correctly inserted loxP sites, using primers P1+P2 for the upstream and P3+P4 for the downstream loxP site. Expression of active Cre resulted in ~40% decrease of KMT2D protein as measured by fluorescent immunocytochemistry, compared to iPSCs treated with inactive ΔCre.

C, Differentiation protocols for generating glutamatergic (Ngn2) and GABAergic (Ascl1 and Dlx2) neurons. iNs were co-cultured with mouse (ms) astrocytes.

E and F, Human *KMT2D*-mutant (Cre) excitatory neurons show a decrease in PSD95 synaptic puncta density but an increase in puncta intensity.

G and H, Mutant (Cre) inhibitory neurons exhibit an increase in vGAT synaptic puncta density.

I, Representative calcium imaging micrographs of cultured wild-type (ΔCre) and mutant (Cre) human iNs overexpressing GCaMP8. Network activity was induced by 2.5 mM KCl and 2 mM $CaCl_2$. Warmer colors indicate higher fluorescence intensity. Arrows highlight active neurons displaying calcium transients.

J, Representative traces of GCamp8 transients showing fluorescence intensity changes (ΔF/F0) over time. Mutant neurons show decreased event frequency.

K-M, Summary graphs of individual neuron firing frequency (C), average firing frequency per view field (D), and signal intensities in single neurons (E).

Data are individual values (one image or video in B, F, G, L; and one cell in K and M) and means ± SEM; statistical significance was assessed by two-tailed unpaired Student's t-test (*, $P < 0.05$; ** $p<0.01$).

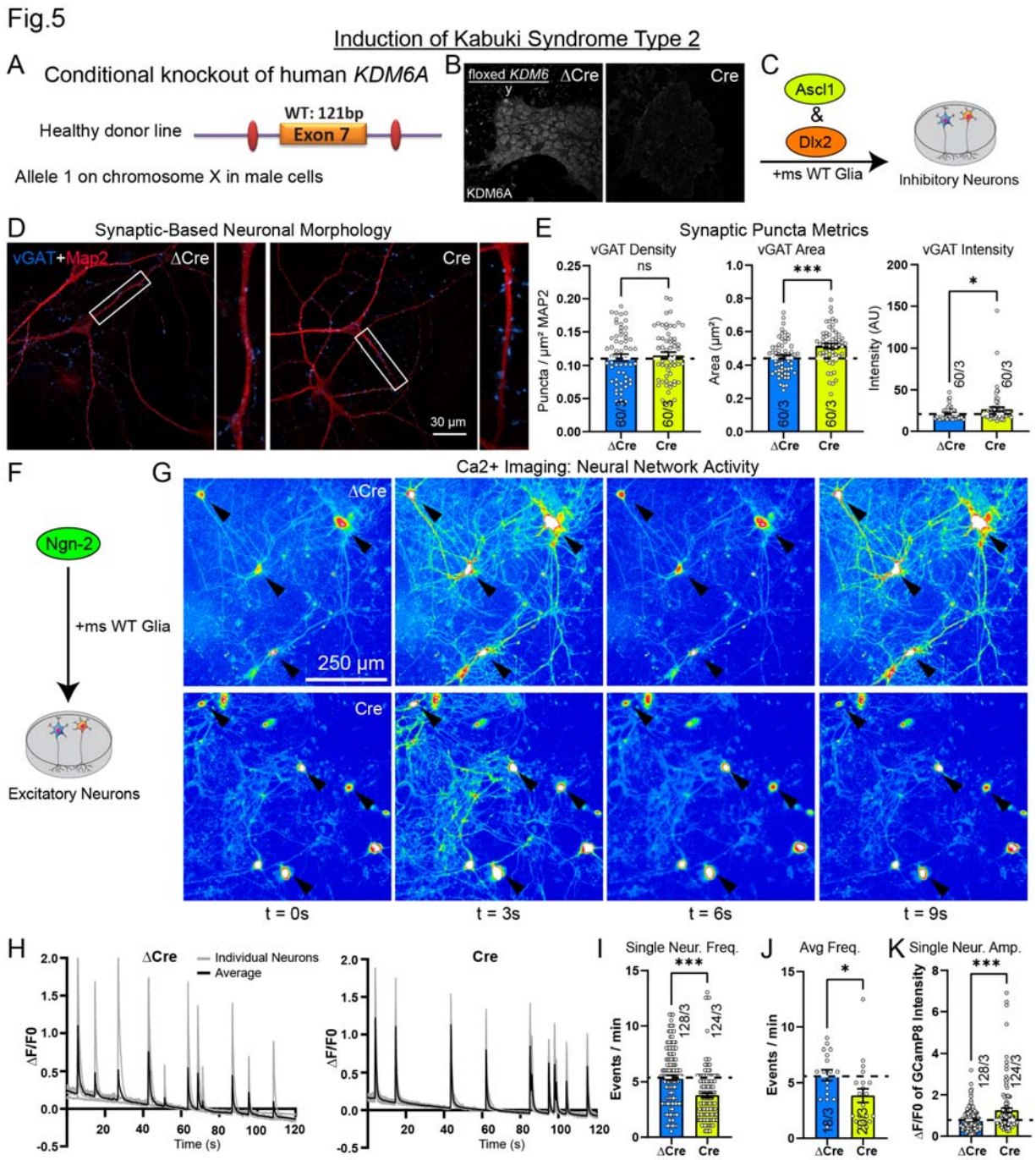

Figure 5: Increased inhibitory synapse development in a human model for Kabuki syndrome type 2

A, Specific heterozygous targeting strategy of X-linked *KDM6A* in iPSCs from a male donor without disease-causing mutations.

B, Expression of active Cre results in loss of KDM6A signal, as measured by fluorescent immunocytochemistry, compared to iPSCs treated with inactive ΔCre.

C-E, Differentiation protocols used for generating GABAergic iNs (overexpression of transcription factors Ascl1 and Dlx2) for subsequent synapse analysis. Mutant (Cre) inhibitory neurons show an increase in vGAT synaptic puncta area and intensity (D and E).

F and G, Differentiation protocols used for generating glutamatergic iNs (overexpression of transcription factor Ngn2) for subsequent calcium imaging. Representative calcium imaging micrographs of wild-type (ΔCre) and mutant (Cre) human iNs overexpressing GCaMP8. Network activity was induced by 8 mM KCl and 4 mM $CaCl_2$. Warmer colors indicate higher fluorescence intensity. Arrows point to active neurons displaying calcium transients.

H, Representative traces of GCaMP8 transients showing fluorescence intensity changes (ΔF/F0) over time. Mutant neurons show decreased event frequency.

I-K, Summary graphs of individual neuron firing frequency (H), average firing frequency per view field (I), and signal intensities in single neurons (J).

Data are presented as individual values (one image or video in E and I; and one cell in H and J) and means ± SEM; statistical significance was assessed by two-tailed unpaired Student's t-test (*, $P < 0.05$; *** $p<0.001$).

Fig.6

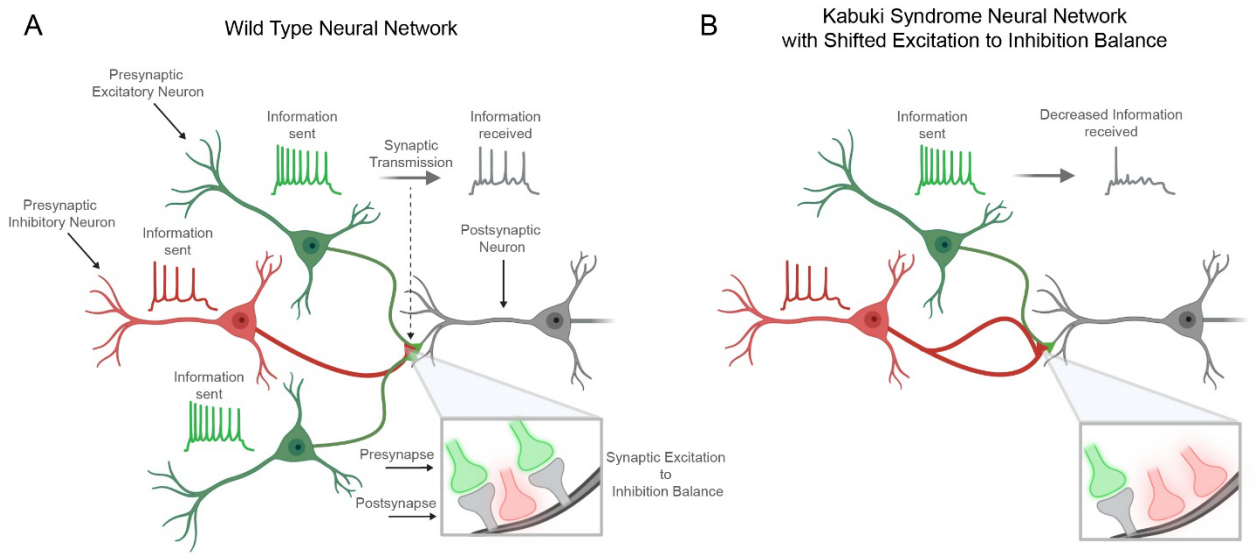

Figure 6: Neural networks in Kabuki syndrome show enhanced inhibitory synaptic development

A, Example network consisting of excitatory (green) and inhibitory neurons (red), promoting and repressing information transfer at synapses (spike diagrams, left vs. right, respectively).

B, Synaptic dysfunction: Due to an overabundance of inhibitory synapses, information transfer through the network is impaired.